Uniformly Semiglobally Exponential Stability of Vector Field Guidance Law and Autopilot for Path-Following

Haitong Xu[a], Thor I. Fossen[b], C. Guedes Soares[a,*]

[a] *Centre for Marine Technology and Ocean Engineering (CENTEC), Instituto Superior Técnico, Universidade de Lisboa, Av. Rovisco Pais, 1049-001 Lisboa, Portugal.*
[b] *Department of Engineering Cybernetics, Norwegian University of Science and Technology, 7491 Trondheim, Norway.*

Abstract

A uniform semiglobal exponential stability (USGES) proof for a time-varying vector field guidance law used for path-following control of vehicles is presented. A sliding mode control is introduced for heading autopilot design and Lyapunov methods are used to derive the control law. The equilibrium point of the autopilot error dynamics is proven to be globally exponentially stable (GES). The main result is a time-varying vector field guidance law in cascade with the autopilot. A theorem ensures that the equilibrium point of the cascaded system is uniformly semiglobally exponentially stable. Both straight-line and curved-path path following scenarios are considered in the presence of ocean currents. Simulation studies are carried out to verify the theoretical results. The time-varying guidance laws can also be applied to vehicles in general such as aircraft, underwater vehicles, drones and autonomous vehicles.

Keywords: Time-varying vector field, Stability analysis, Path following, Cascaded theory, Kinematics

*Corresponding author
Email addresses: haitong.xu@centec.tecnico.ulisboa.pt (Haitong Xu), thor.fossen@ntnu.no (Thor I. Fossen), c.guedes.soares@centec.tecnico.ulisboa.pt (C. Guedes Soares)

1. Introduction

Autonomous vehicles will have broad application prospects in the future maritime industry. They are able to perform advanced operations and tasks in dangerous or inaccessible places. Consequently, they have been widely used both in navy applications and even some commercial applications such as marine survey, coast patrol, inspection and operation of underwater production system. Guidance systems are critically important for the overall performance and safety of autonomous vehicles [1], because they are concerned with the transient motion behavior associated with the achievement of motion control scenarios such as path following [2, 3], path tracking [4], and path maneuvering [5].

For path-following control, the objective is to follow a predefined path, which usually is specified by waypoints [6]. Raffo *et al*, [7] introduced a nonlinear robust control strategy designed for underactuated mechanical systems for the path tracking problem of a quadrotor unmanned aerial vehicle. Parametric uncertainties of path-following control for articulated heavy-duty vehicles was studied by Barbosa*et al*, [8]. Zheng *et al*, [9], presented a novel path following control method for autonomous airship and proved that the controlled closed-loop system is asymptotically stable. Line-of-Sight (LOS) is a popular and effective guidance law for autonomous marine vehicles and its properties have been studied thoroughly in the literature, see [10, 11, 12, 13, 14, 15]. Classical LOS methods usually rely on a constant look-ahead distance by mimicking an experienced sailor. LOS with a time-varying look-ahead distance, which depends on the cross-track error was introduced by Lekkas *et. al* [16], and a dynamic version of LOS can also be found in [17]. Recently, an integral LOS (ILOS) has been proposed and extensively analyzed. It embeds an integral term that compensates the transverse disturbance [3, 18, 19, 20]. A conceptual new ILOS based on adaptive control theory was proposed by Fossen and Lekkas in [2] and it can compensate the drift forces effectively.

The stability analysis is an important and challenging topic for guidance and control systems when used in autonomous marine vehicles. Do *et al.*,[21], proposed a robust adaptive controller for underactuated ships. Stability analysis and experiments of path-following for a underactuated ship were given in Refs. [22, 23]. Global exponential stable (GES) is usually the most desired quality of a closed-loop control system [24][25] since it guarantees additional robustness and performance properties. However, it cannot be achieved for certain nonlinear system due to hard kinematic nonlinearities and singularities. For LOS guidance problems, it is well known that the kinematics introduces saturation through the trigonometric functions [26]. Global *κ-exponential stability* as defined by Sørdalen and Egeland [27] was first proven for these problems and later by Pettersen and Lefeber [28] who used a simplified vehicle model. This work has been further extended to a more complex ship model [29, 30]. More recently, the stability results were strengthen to uniform semiglobal exponential stability (USGES) by Fossen and Pettersen [26]. USGES is very important for the robustness of a system with environmental disturbance. It is slightly weaker than GES but stronger than global κ-exponential stability. Chaillet and Loria, [31], presented sufficient conditions for a cascade composed of nonlinear time-varying systems that are uniformly globally practically asymptotically stable. Lyapunov sufficient conditions for USGES of nonlinear time-varying systems were presented by Fossen and Pettersen [26], and its robustness properties were also discussed in [32].

The vector field guidance law is a standard method and is widely used for unmanned aerial vehicles (UAVs). In [33], global stability of a vector field guidance law was proven using Lyapunov techniques. Global uniform bounded stability of the vector field path-following system for arbitrary curves was presented in [34]. Nelson *et al.* [35] proposed a vector field guidance law for a small unmanned air vehicle and global asymptotic stability was proven. Recently, Xu and Guedes Soares,[36] employed a vector field guidance law for path-following control of underactuated marine vehicles, where the nonlinear maneuvering model was estimated using system identification [37]. A comparison between the ILOS guidance and the vector field guidance for an underwater vehicle was presented by Caharija *et al.* [38].

The nonlinear controller for ship motion control was summarized in [39], where a brief history of model based ship control system was presented. Recently, many works on nonlinear controller for autopilot or motion control of marine vessel have been reported. Oh and Sun [40] presented a model predictive control (MPC) for a way-point tracking of underactuated surface vessels. Guerrero *et al* [41] employed an adaptive high order sliding mode controller for trajectory tracking of autonomous underwater vehicle. Yu *et al* [42] used a fuzzy adaptive control for bottom following of an autonomous underwater vehicle subject to input saturation. A review on fuzzy logic-based guidance and control for marine robotic vehicles was given by Xiang*et al*,[43]. Sørensen and Breivik, [44] evaluated the adaptive controllers for path-following control of marine surface ship. Angelo *et al* [45] focused on the smooth behaviors when the autopilot of a marine vessel switching among different controllers in a complex maneuvering operation.

The main contribution of this paper is to propose a novel time-varying vector field guidance law for which a proof is given that the equilibrium point of the time-varying vector field guidance law in cascade with a heading autopilot is USGES using cascaded theory. To the authors' best knowledge only global asymptotic stability of the vector field guidance law has so far been proven in the literature. The proposed vector field guidance law of this article is, however, proven to yield USGES for straight lines and the result is also generalized to curved paths. In order to obtain a cascaded system structure, a sliding mode control is used for heading autopilot design. A Control Lyapunov Function (CLF) is employed to derive the control law, which guarantees that the equilibrium point of the subsystem is GES. Using cascaded theory, it is then possible to show USGES of the whole system. Finally, in order to evaluate the performance and robustness of the proposed time-varying vector field guidance law, both straight-line and curved-line path following problems are studied under the influence of ocean currents.

The structure of this paper is as follows: Section 2 is a brief introduction to the kinematics of path-following control problems. Section 3 offers a detailed description of a time-varying vector field guidance law. In section 4, a heading autopilot using sliding mode control is presented, and the control law is derived using a CLF and GES of the subsystem is proven. In section 5, a theorem is developed to guarantee USGES of the nonlinear time-varying cascaded system and the detailed proof is also given in this section. Finally, in section 6 the conclusions are presented.

2. Kinematics

A closed-loop guidance and control system for a marine craft is shown in Figure 1, where the crab angle β is directly measured [20]. The waypoints are assumed to be specified by an operator. In this section, the kinematics of two-dimensional path-following guidance problems is briefly reviewed. Two-dimensional path following is standard in the literature, because a three-dimensional path-following problem can be solved independently in the horizontal and vertical planes. A marine craft is assumed to follow a predefined straight or curved path as showed in Figure 2. Three frames are defined in Figure 2. For example, the curved path is defined in the North-East-Down (NED) frame. The body-fixed frame is a moving coordinate frame that is fixed to the craft. The origin of the body-fixed frame coincides with the centre of gravity. The path-tangential frame is a moving coordinate frame, whose origin is the projection of the ship's centre of gravity.

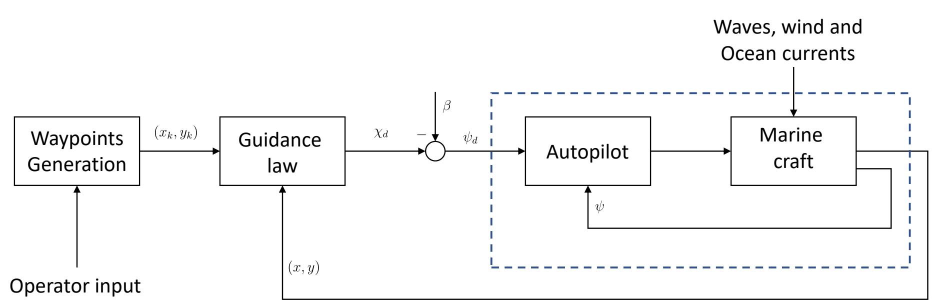

Figure 1: A typical guidance and control system for marine craft, where the crab angle β can be compensated [20].

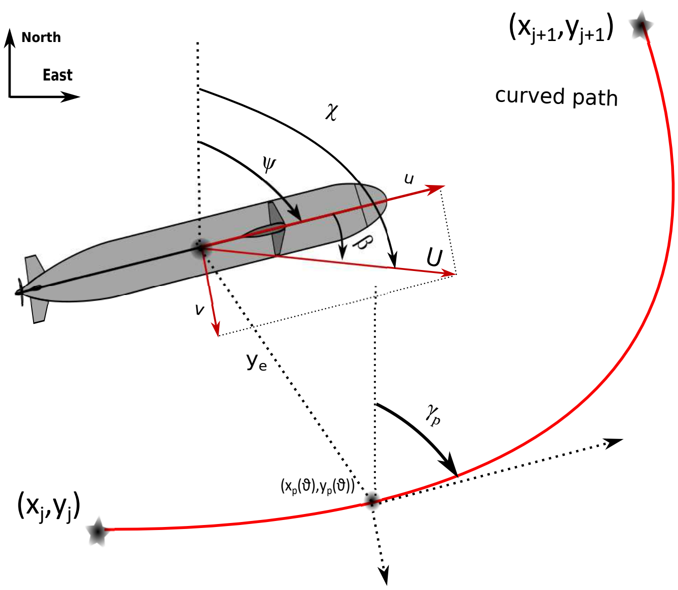

Figure 2: Geometrical description of the path-following control problem.

2.1. Cross-track error

Consider a marine craft moving in a horizontal plane, a two dimensional continuous $\mathbb{C}^1$ path was predefined as $(x_p(\theta), y_p(\theta))$, where θ is the variable. The path is assumed to go through the predefined waypoints (x_j, y_j) for $j = 1, ..., N$. The path variable θ propagates according to Fossen [6]:

$$\dot{\theta} = \frac{U}{\sqrt{x_p'(\theta)^2 + y_p'(\theta)^2}} \tag{1}$$

where, U is the speed over ground, $U = \sqrt{u^2 + v^2}$. the path tangential angle $\gamma_p(\theta)$ is defined by $(x_p'(\theta), y_p'(\theta))$, as

$$\gamma_p(\theta) = \text{atan2}(y_p'(\theta), x_p'(\theta)) \tag{2}$$

where, $(y_p'(\theta), x_p'(\theta))$ is the first derivative at the point $(y_p(\theta), x_p(\theta))$. Hence, the path-tangential reference frame can be found by rotating an angle $\gamma_p(\theta)$ in NED reference frame using the rotation matrix:

$$\boldsymbol{R}(\gamma_p(\theta)) = \begin{bmatrix} \cos(\gamma_p(\theta)) & -\sin(\gamma_p(\theta)) \\ \sin(\gamma_p(\theta)) & \cos(\gamma_p(\theta)) \end{bmatrix} \in \boldsymbol{SO}(2) \tag{3}$$

where, $\boldsymbol{SO}(2)$ is the special orthogonal group in dimension 2. By inspection of Figure 2, the cross-track error can be calculated using (4):

$$\begin{bmatrix} 0 \\ y_e \end{bmatrix} = \boldsymbol{R}(\gamma_p(\theta)) \begin{bmatrix} x - x_p(\theta) \\ y - y_p(\theta) \end{bmatrix} \tag{4}$$

where (x, y) is the ship's position, $(x_p(\theta), y_p(\theta))$ is the origin of the path-tangential reference frame. Expanding (4) leads to the normal line:

$$\frac{y - y_p(\theta)}{x - x_p(\theta)} = -\frac{1}{\tan\big(\gamma_p(\theta)\big)} \tag{5}$$

and the cross-track error:

$$y_e = -\big(x - x_p(\theta)\big)\sin(\gamma_p(\theta)) + \big(y - y_p(\theta)\big)\cos\big(\gamma_p(\theta)\big) \tag{6}$$

As pointed by Fossen [2] and Samson [46], if the path is a closed curve, then there will be infinite solutions of (5). Consequently, it is necessary to assume that the path is an open curve. This means that the end point is different from the initial point. A unique solution needs to be defined, for instance using the result of Fossen and Pettersen [26].

$$\begin{aligned} \theta^* &:= \arg \underbrace{\min}_{\theta \geq 0} \left\{ \frac{U^2}{x_p'(\theta)^2 + y_p'(\theta)^2} \right\} \\ &\text{Subject to (5)} \end{aligned} \tag{7}$$

This is a nonlinear optimization problem, which can be solved numerically. In practice, the candidate that is closest to the previous θ^*, will be chosen from the all possible solutions $\theta_i (i = 1, ..., M)$ given by (5).

2.2. Kinematic equations

As presented in Chapter 2 of Fossen [6], the velocity of *surge, sway* and *yaw*, (u, v and r) can be used to describe the kinematic equations of a marine vessel:

$$\begin{aligned} \dot{x} &= u\cos(\psi) - v\sin(\psi) \\ \dot{y} &= u\sin(\psi) + v\cos(\psi) \\ \dot{\psi} &= r \end{aligned} \tag{8}$$

where ψ is the heading or yaw angle, which can be measured using a compass. Differentiation of (6) yields:

$$\begin{aligned} \dot{y}_e = & \underbrace{-\left(\dot{x} - \dot{x}_p\left(\theta\right)\right)\sin\left(\gamma_p\left(\theta\right)\right) + \left(\dot{y} - \dot{y}_p\left(\theta\right)\right)\cos\left(\gamma_p\left(\theta\ \right)\right)}_{Term1} \\ & - \underbrace{\left(\left(x - x_p\left(\theta\right)\right)\cos\left(\gamma_p\left(\theta\right)\right) + \left(y - y_p\left(\theta\right)\right)\sin\left(\gamma_p\left(\theta\right)\right)\right)\dot{\gamma}_p(\theta)}_{Term2} \end{aligned} \tag{9}$$

Hence, by substituting (5) into *Term 2*, the second line cancels. *Term 1* can be simplified due to the definition of $\gamma_p(\theta)$ in (2). Substitution of (8) into the time differentiated cross-track error (9) gives:

$$\begin{aligned} \dot{y}_e &= -\dot{x}\sin\left(\gamma_p\left(\theta\right)\right) + \dot{y}\cos\left(\gamma_p\left(\theta\right)\right) \\ &= -\left(u\cos\left(\psi\right) - v\sin\left(\psi\right)\right)\sin\left(\gamma_p\left(\theta\right)\right) \\ &+ \left(u\sin\left(\psi\right) + v\cos\left(\psi\right)\right)\cos\left(\gamma_p\left(\theta\right)\right) \\ &= U\sin\left(\psi - \gamma_p\left(\theta\right) + \beta\right) \end{aligned} \tag{10}$$

where the amplitude $U = \sqrt{u^2 + v^2}$ is the ground speed of a ship, which can be directly measured using GNSS. The phase $\beta = \text{atan2}(v, u)$ is recognized as the *crab angle*. It is the difference in heading angle ψ and course angle χ. Moreover,

$$\chi = \psi + \beta \tag{11}$$

Finally, the differential equation for y_e becomes:

$$\dot{y}_e = U\sin\left(\chi - \gamma_p\left(\theta\right)\right) \tag{12}$$

3. Time-varying vector field guidance law

The objective of this section is to propose a guidance law for accurate path following for autonomous vessels. The vector field guidance law calculates a vector field around the predefined path to be tracked. Figure 3 provides an illustration to understand how a vector field guidance law can be used for path following control. In Figure 3, the vectors in the field are directed toward the

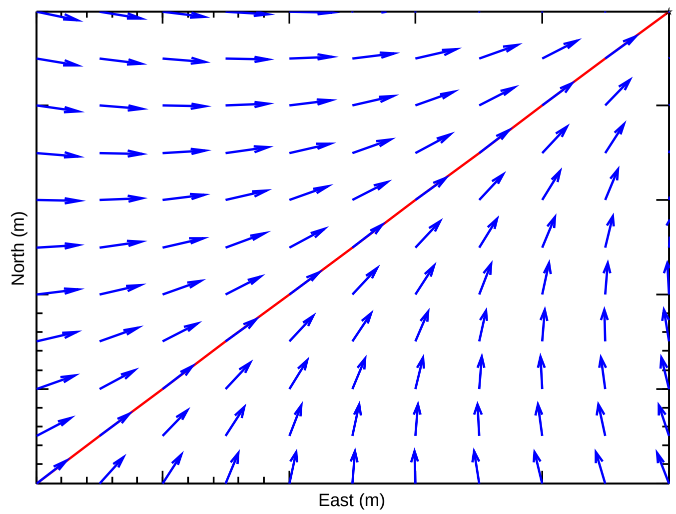

Figure 3: Vectors around the path, generated by using the vector field guidance law.

path to be followed. They indicate the desired direction of vessel, and serve as course commands to the autonomous vessel.

The following time-varying vector field guidance law is proposed:

$$\begin{aligned}\chi_d = \psi_d + \beta &= \gamma_p - \tan^{-1}\left(\operatorname{sgn}(y_e)\left(\frac{|y_e|}{\Delta}\right)^{\theta(t,y_e)}\right)\\ &= \gamma_p - \operatorname{sgn}(y_e)\tan^{-1}\left(\left(\frac{|y_e|}{\Delta}\right)^{\theta(t,y_e)}\right)\end{aligned} \tag{13}$$

where, $\operatorname{sgn}(\cdot)$ is the signum function. $\theta(t, y_e)$ is a time-varying function to be defined later and $\Delta > 0$ is a pre-defined constant. The course angle tracking error satisfies:

$$\tilde{\chi} = \chi - \chi_d = \psi - \psi_d = \tilde{\psi} \tag{14}$$

Substituting (13) and (14) into (12) gives:

$$\dot{y}_e = U\sin\left(\tilde{\psi} - \operatorname{sgn}(y_e)\tan^{-1}\left(\left(\frac{|y_e|}{\Delta}\right)^{\theta(t,y_e)}\right)\right) \tag{15}$$

Using the property, $\sin(a+b) = \sin(a)\cos(b) + \cos(a)\sin(b)$, gives:

$$\begin{aligned} \dot{y}_e = U \sin\left(\tilde{\psi}\right) \cos\left(\tan^{-1}\left(\left(\frac{|y_e|}{\Delta}\right)^{\theta(t,y_e)}\right)\right) \\ - \operatorname{sgn}(y_e)\, U \cos(\tilde{\psi}) \sin\left(\tan^{-1}\left(\left(\frac{|y_e|}{\Delta}\right)^{\theta(t,y_e)}\right)\right) \end{aligned} \tag{16}$$

which can be simplified by using the trigonometry equation, $\sin\left(-\tan^{-1}(x)\right) = x/\sqrt{1+x^2}$. Moreover,

$$\begin{aligned} \dot{y}_e &= U \sin(\tilde{\psi}) \frac{\Delta^{\theta(t,y_e)}}{\sqrt{\Delta^{2\theta(t,y_e)} + |y_e|^{2\theta(t,y_e)}}} \\ &\quad - \operatorname{sgn}(y_e)\, U \cos(\tilde{\psi}) \frac{|y_e|^{\theta(t,y_e)}}{\sqrt{\Delta^{2\theta(t,y_e)} + |y_e|^{2\theta(t,y_e)}}} \\ &= \underbrace{-\operatorname{sgn}(y_e) \frac{U|y_e|^{\theta(t,y_e)}}{\sqrt{\Delta^{2\theta(t,y_e)} + |y_e|^{2\theta(t,y_e)}}}}_{f_1(t,y_e)} + \underbrace{U\phi\left(t, y_e, \tilde{\psi}\right)}_{g\left(t,y_e,\tilde{\psi}\right)} \tilde{\psi} \end{aligned} \tag{17}$$

where $\phi(t, y_e, \tilde{\psi})$ is defined as:

$$\begin{aligned} \phi\left(t, y_e, \tilde{\psi}\right) := \frac{\sin\left(\tilde{\psi}\right)}{\tilde{\psi}} \frac{\Delta^{\theta(t,y_e)}}{\sqrt{\Delta^{2\theta(t,y_e)} + |y_e|^{2\theta(t,y_e)}}} \\ - \operatorname{sgn}(y_e) \frac{\cos\left(\tilde{\psi}\right) - 1}{\tilde{\psi}} \frac{|y_e|^{\theta(t,y_e)}}{\sqrt{\Delta^{2\theta(t,y_e)} + |y_e|^{2\theta(t,y_e)}}} \end{aligned} \tag{18}$$

Assume that $0 < \Delta_{min} < \Delta < \Delta_{max}$. Hence, the function $\phi(t, y_e, \tilde{\psi}) \leq c$ for all y_e and $\tilde{\psi}$, because $\left|\frac{\sin(x)}{x}\right| \leq 1$, and $\left|\frac{(\cos(x)-1)}{x}\right| \leq 0.73$, then

$$\begin{aligned} \left|\frac{\Delta^{\theta(t,y_e)}}{\sqrt{\Delta^{2\theta(t,y_e)} + |y_e|^{2\theta(t,y_e)}}}\right| \leq 1 \\ \left|\frac{|y_e|^{\theta(t,y_e)}}{\sqrt{\Delta^{2\theta(t,y_e)} + |y_e|^{2\theta(t,y_e)}}}\right| \leq 1 \end{aligned} \tag{19}$$

Consequently, it can be concluded that $\phi(t, y_e, \tilde{\psi})$ is upper bounded.

4. Heading autopilot design

In this section, the nonlinear sliding mode controller is used for heading autopilot design in order to obtain strong stability properties. The Nomoto model is chosen because it is widely used for the describe the yaw dynamics of a marine vessel [6, 47]. It was used to design the nonlinear ship steering system [48]. Consider,

$$\begin{aligned} \dot{\psi} &= r \\ T\dot{r} + r &= K\delta + b_0 \end{aligned} \tag{20}$$

where, T and K are the Nomoto time and gain constants, respectively. $b_0 \leq b_{max}$ represents a bounded bias term due to environmental disturbance and unmodeled dynamics. δ is the rudder deflection angle. Note that $\tilde{\chi} = \tilde{\psi}$ so it is sufficient to analyze the heading error dynamics, which is expressed in terms of the sliding surface:

$$s := \dot{\tilde{\psi}} + 2\lambda\tilde{\psi} + \lambda^2 \int_0^t \tilde{\psi}(\tau)\, d_\tau := \dot{s}_0 + \lambda s_0 \tag{21}$$

where $s_0 = \tilde{\psi} + \lambda \int_0^t \tilde{\psi}(\tau) d_\tau$ and λ is a design constant, which reflects the bandwidth of the controller [6]. The error dynamics can be expressed in state-space form as:

$$\begin{bmatrix} \dot{\tilde{\psi}} \\ \dot{s}_0 \end{bmatrix} = \underbrace{\begin{bmatrix} -\lambda & -\lambda \\ 0 & -\lambda \end{bmatrix}}_{\boldsymbol{A}} \begin{bmatrix} \tilde{\psi} \\ s_0 \end{bmatrix} + \underbrace{\begin{bmatrix} 1 \\ 1 \end{bmatrix}}_{\boldsymbol{b}} s \tag{22}$$

Define the signal $r_r := r - s$, and substitute into (20) gives:

$$T\dot{s} + s = K\delta - T\dot{r}_r - r_r + b_0 \tag{23}$$

Then the heading controller can be chosen as:

$$\delta = \frac{1}{K}\left(T\dot{r}_r + r_r - K_d s - \eta \operatorname{sgn}(s)\right) \tag{24}$$

where $K_d > 0$ is the feedback control gain, which is used to speed up the convergence of the tracking error s to zero. $\eta \geq b_{max}$ is a positive design gain, which is determined by Lyapunov stability analysis [49]. It is well known that the switching term $\eta\text{sgn}(s)$ can lead to chattering. Hence, a signum function, $\eta\tanh(\cdot)$, will used in Eq.24, as it serves as a low-pass filter and diminishes the chattering. Consider the CLF

$$V_2 = \boldsymbol{x}^T \boldsymbol{P} \boldsymbol{x} + \frac{1}{2} T s^2 \tag{25}$$

where $\boldsymbol{x} = [\tilde{\psi}, s_0]^T$ and $\boldsymbol{P} = \boldsymbol{P}^T > 0$ is given by

$$\boldsymbol{PA} + \boldsymbol{A}^T \boldsymbol{P} = -q\boldsymbol{I} \tag{26}$$

Here $q > 0$ is a specified constant. Hence, it follows that:

$$\begin{aligned} \dot{V}_2 &= \boldsymbol{x}^T \left(\boldsymbol{A}^T \boldsymbol{P} + \boldsymbol{PA} \right) \boldsymbol{x} + 2\boldsymbol{x}^T \boldsymbol{Pb} s \\ &- (1 + K_d)\, s^2 + b_0 s - \eta |s| \\ &\le -q\|\boldsymbol{x}\|^2 + 2\|\boldsymbol{P}\|\|\boldsymbol{x}\||s| - (1 + K_d)\, s^2 \end{aligned} \tag{27}$$

From (27), the feedback control gain, K_d, need to be carefully chosen in order to ensure that $\dot{V}_2 < 0$. Assume $\lambda_{max}(\boldsymbol{P})$ is the maximum eigenvalue of $\boldsymbol{P}$.

$$\begin{bmatrix} q & -\lambda_{max}(\boldsymbol{P}) \\ -\lambda_{max}(\boldsymbol{P}) & 1 + K_d \end{bmatrix} > 0 \tag{28}$$

Then the control gain can be defined as $K_d > \lambda_{max}(\boldsymbol{P})^2/q - 1 > 0$, which clearly implies that $\dot{V}_2$ is negative. Hence, the equilibrium point $[\tilde{\psi}, s_0]^T = \boldsymbol{0}$ is GES (Theorem 4.10 in [24]). As shown by Bhat and Bernstein [50], mechanical systems with rotational degrees of motion cannot be globally stabilized by continuous feedback due to the topological obstruction imposed by $SO(3)$. Hence, the GES property is based on the assumption that $\tilde{\psi} \in \text{R}$ and not $(-pi, pi]$. However, if $\tilde{\psi}$ is mapped to $(-pi, pi]$ when implementing the autopilot, this still guarantees local exponential stability [51, 52]. As discussed in [2], it is practical to treat K_d and η as tunable parameters, because it is easy to satisfy the gain requirements for a marine craft described by the Nomoto model.

5. Stability of the nonlinear time-varying cascaded system

The stability proof of the coupled guidance and control system is presented in this section. As can be observed from Eq. (29), the y_e dynamic equation is

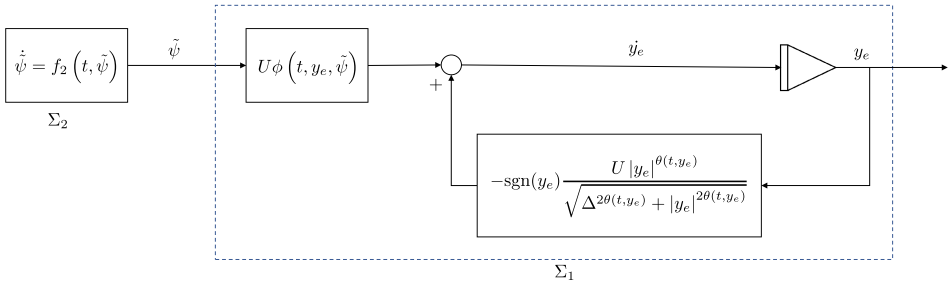

Figure 4: Error dynamics of the cascaded system, which is described by (29) and (31)

.

discontinuous. Non-smooth Lyapunov function are believed to be natural for non-smooth dynamic systems [53], but, indeed, this will result a new source of discontinuity, and complicate the stability analysis. Wu *et al.* [54] suggested to first consider the construction of smooth Lyapunov functions before resorting to non-smooth ones. The smooth Lyapunov function also works for the present dynamic equation, and more details can be found in Refs.[55, 56, 54] If the guidance law (13) is chosen, the cross-track error (17) forms a nonlinear time-varying cascaded system with the heading autopilot system in Section 3 as shown in Figure 4.

The overall system is a cascade system:

$$\Sigma_1 : \dot{y}_e = \underbrace{-\mathrm{sgn}\left(y_e\right) \frac{U|y_e|^{\theta(t,y_e)}}{\sqrt{\Delta^{2\theta(t,y_e)} + |y_e|^{2\theta(t,y_e)}}}}_{f_1(t,y_e)} \tag{29}$$

$$+ \underbrace{U\phi(t, y_e, \tilde{\psi})}_{g(t,y_e,\tilde{\psi})}\tilde{\psi} \tag{30}$$

$$\Sigma_2 : \quad \dot{\tilde{\psi}} = f_2(t, \tilde{\psi}) \tag{31}$$

where $f_2(t, \tilde{\psi})$ defines the heading tracking error dynamics as outlined in Section 4. The vehicle dynamics along with the heading controller is the driving system Σ_2 and the vehicle in combination with the time-varying vector field guidance law constitutes the driven system Σ_1. The yaw angle tracking error affects the convergence of the guidance system's objective, which is to minimize the cross-track error y_e.

Definition. The time varying function $\theta(t, y_e)$ is non-decreasing and positive semi definite, i.e. $\theta(t, y_e = 0) \geq 1$. Furthermore,

$$\theta'(t, y_e) \geq 0 \tag{32}$$

Property. The time-varying function $\theta(t, y_e)$ guarantees that the function $g(t, y_e) = |y_e|^{\theta(t,y_e)-1}$ is continuous positive defined and lower bounded. Moreover,

$$0 \leq C_r \leq g(t, y_e) \tag{33}$$

The main result of the paper is formulated in Theorem, which guarantees that the cascade system (29)–(31) of the time-varying vector fields guidance law and heading autopilot is USGES.

Theorem. Assume the control law (24) is used to stabilize the system Σ_2, and that the guidance law (13) specifies the desired heading ψ_d angle for the system Σ_1. Then the equilibrium point $(y_e, \tilde{\psi}) = (0, 0)$ of the system (29)–(31) is USGES, if the function $\theta(t, y_e)$ satisfies the *Property*, and the predefined parameter Δ satisfies $0 < \Delta_{min} < \Delta < \Delta_{max}$ for speeds $0 < U_{min} < U < U_{max}$.

Proof. As shown in Section 3, the equilibrium point $\tilde{\psi} = 0$ and thus $\tilde{\chi} = 0$ of the heading autopilot system Σ_2 given by (31) is GES. The nominal system (Σ_1 system with $\tilde{\psi} = 0$) is:

$$\dot{y}_e = -\mathrm{sgn}\,(y_e)\, \frac{U|y_e|^{\theta(t,y_e)}}{\sqrt{\Delta^{2\theta(t,y_e)} + |y_e|^{2\theta(t,y_e)}}} \tag{34}$$

The system (34) is nonautonomous since the function $\theta(t, y_e)$ is time-varying. Consider the CLF:

$$V_1(t, y_e) = \frac{1}{2} y_e^2 \tag{35}$$

where $V_1(t, y_e) > 0$ if $y_e \neq 0$. The time derivative is:

$$\begin{aligned} \dot{V}_1(t, y_e) &= -\mathrm{sgn}\,(y_e)\, y_e \frac{U|y_e|^{\theta(t,y_e)}}{\sqrt{\Delta^{2\theta(t,y_e)} + |y_e|^{2\theta(t,y_e)}}} \\ &= -\frac{U|y_e|^{\theta(t,y_e)+1}}{\sqrt{\Delta^{2\theta(t,y_e)} + |y_e|^{2\theta(t,y_e)}}} \leq 0 \end{aligned} \tag{36}$$

since $V_1(t, y_e) > 0$ and $\dot{V}_1(t, y_e) \le 0$, according to the Theorem 4.8 by Khalil [24], the equilibrium point is uniformly stable. Moreover,

$$\left|y_e(t)\right| \le \left|y_e(t_0)\right|, \qquad \forall t \ge t_0 \tag{37}$$

Rewriting (36) as in (39), and defining $\Phi(t, y_e)$ as:

$$\Phi(t, y_e) := \frac{U|y_e|^{\theta(t,y_e)-1}}{\sqrt{\Delta^{2\theta(t,y_e)} + |y_e|^{2\theta(t,y_e)}}} \tag{38}$$

gives

$$\dot{V}_1(t, y_e) = -\Phi(t, y_e) y_e^2 \tag{39}$$

For $\forall y_e \in B_r$, (where $B_r = \{x \in B_r \,:\, \|x\| \le r\}$), and from the *Property* it then follows that:

$$\begin{aligned} \Phi(t, y_e) &= \frac{U|y_e|^{\theta(t,y_e)-1}}{\sqrt{\Delta^{2\theta(t,y_e)} + |y_e|^{2\theta(t,y_e)}}} \\ &\ge \frac{U_{\min} C_r}{\sqrt{\Delta_{\max}^{2\theta(t_0,r)} + r^{2\theta(t_0,r)}}} := c(r) \end{aligned} \tag{40}$$

Then

$$\dot{V}_1(t, y_e) = -2\Phi(t, y_e) V_1(t, y_e) \le -2c(r) V_1(t, y_e), \forall y_e \in B_r \tag{41}$$

Considering (37), the above equation holds for all trajectories generated by the initial conditions $y_e(t_0)$. Using the comparison lemma (Lemma 3.4 by Khalil [24]), Eq. (41) has the solution $V_1(t, y_e) \le e^{-2c(r)(t-t_0)} V_1(t_0, y_e(t_0))$. therefore,

$$y_e(t) \le e^{-c(r)(t-t_0)} y_e(t_0), \forall t \ge t_0 \,\text{and}\, \forall y_e(t_0) \in B_r \tag{42}$$

Hence, it can be concluded that the equilibrium point $y_e = 0$ of the nominal system is USGES (Definition 2.7 by Loria [25]). Finally, under the *Property*, the equilibrium point $(y_e = 0, \tilde{\psi} = 0)$ of the cascaded system described by (29)–(31) is USGES [26, 57, 58, 59]. □

Remark 1. The convergence parameter $c(r)$ depends on the time varying function $\theta(t, y_e)$. The value of $\theta(t, y_e)$ should increase with the cross-track error, y_e. This ensures that the system has a higher converging rate when the cross-track error is large.

Table 1: The principle particularities of “Esso Osaka” ship model .

Parameter	Value	Unite
Length Between perpendiculars	3.250	m
Breadth	0.530	m
Draft	0.217	m
Block coefficient	0.831	
Number of rudder	1	
Rudder area	0.0120	m^2
Propeller area	0.0065	m^2
Longitudinal CG	0.103	m
Displacement	319.40	kg

Remark 2. USGES is slightly weaker than GES, but in this case, GES cannot be achieved due to the definition of the cross-track error dynamics (12), which is saturated due to the sinusoidal function.

6. Simulation study of an underactuated ship

In order to evaluate and compare the performance and robustness during path following both straight lines and a curved path are used in the simulation study. The ship considered is the 3-DOF (surge, sway and yaw) nonlinear mathematical model of “Esso Osaka”. The scaled ship model is $3.25m$ length and with one propeller and one rudder. It is a typical underactuated system. This model is quite comprehensive and it gives highly realistic results [60]. System identification method was used to estimate the hydrodynamic coefficients based on manoeuvring tests[61][]. More details about the mathematical model and hydrodynamic coefficients can be found in [61].

The goal is to follow a trajectory, that is specified in terms of waypoints. The waypoints are defined in Cartesian coordinates and their values are: $\mathrm{wpt}_1 = (40, 20)$, $\mathrm{wpt}_2 = (120, 25)$, $\mathrm{wpt}_3 = (160, 18)$, $\mathrm{wpt}_4 = (200, 22)$, $\mathrm{wpt}_5 = (280, 5)$,

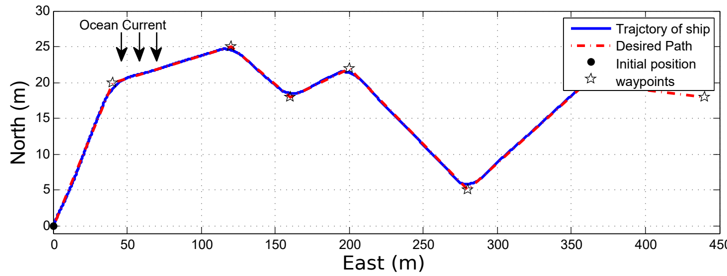

(a) Straight path case

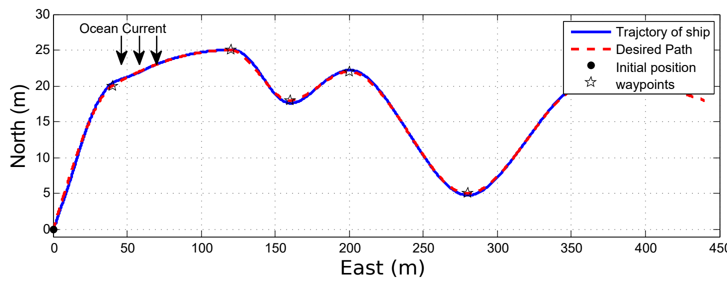

(b) Curved path case

Figure 5: Path following of the underactuated ship using time-varying Vector Field guidance law in the presence of ocean currents. In this case, $U_c = 0.4$ m/s, $\beta = 180$ deg, and $\Delta = 2L_{pp}$.

$\text{wpt}_6 = (360, 20)$, and $\text{wpt}_7 = (440, 18)$ where the units are meters. The straight path is obtained by connecting the adjacent waypoints with a straight line directly, and the curved path is generated using cubic Hermite spline interpolation (CHSI), see [20]. The geometrical information of the predefined paths and the ocean current are presented in Figure 5. It is also seen that the curved path can connect the predefined waypoints successfully. Without loss of generality, the initial position of the ship is assumed to be the origin. During the simulation, the ship moves under the influence of an ocean current with constant magnitude and direction ($U_c = 0.4$ m/s and $\beta_c = 180$ deg) in the NED frame. The rudder saturation ($\delta \leq 35$ deg) and the initial conditions are given: $U_0 = 0.41$ m/s, $\psi_0 = 26$ deg and $r_0 = 0$. The desired speed is kept constant during the simulation.

The heading controller parameters are selected: $K_d = 0.4$, $\eta = 1$ and $\lambda = 0.1$. The time-varying function has been chosen as: $\theta(t, y_e) = 0.4\,|y_e| + 1$, while the

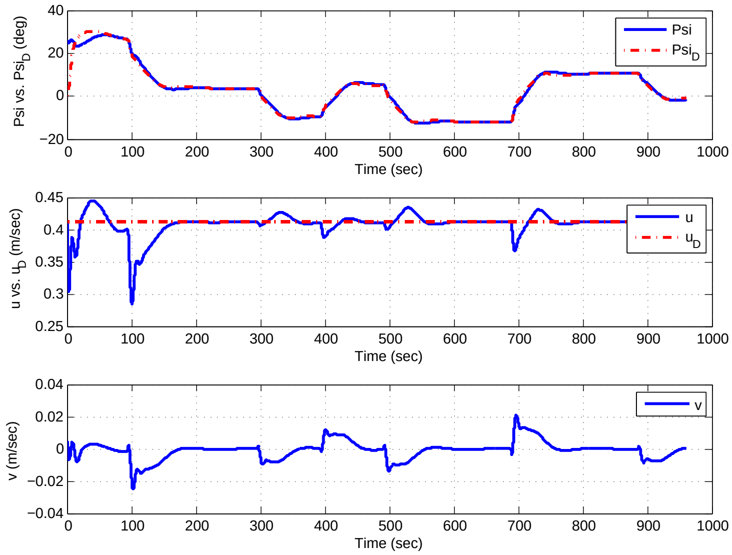

(a) Straight path case

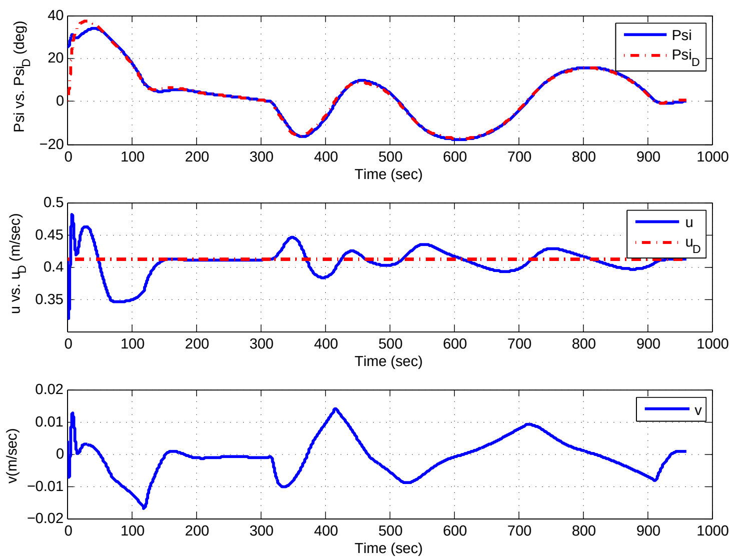

(b) Curved path case

Figure 6: Heading angle, Surge speed (desired versus true) and sway speed from the simulations.

time-varying vector field guidance law is given by (43). The time-varying function increases with y_e, and the function, $g(t, y_e) = |y_e|^{\theta(t,y_e)-1} = |y_e|^{0.4|y_e|} \geq$

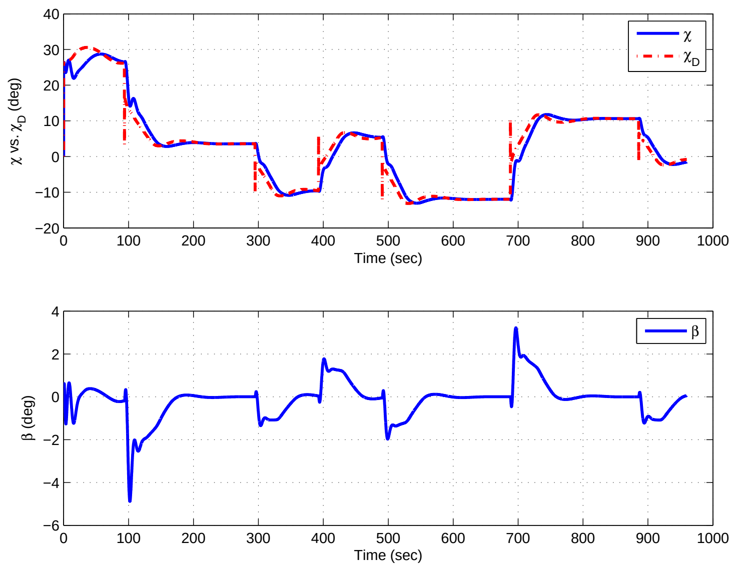

(a) Straight path case

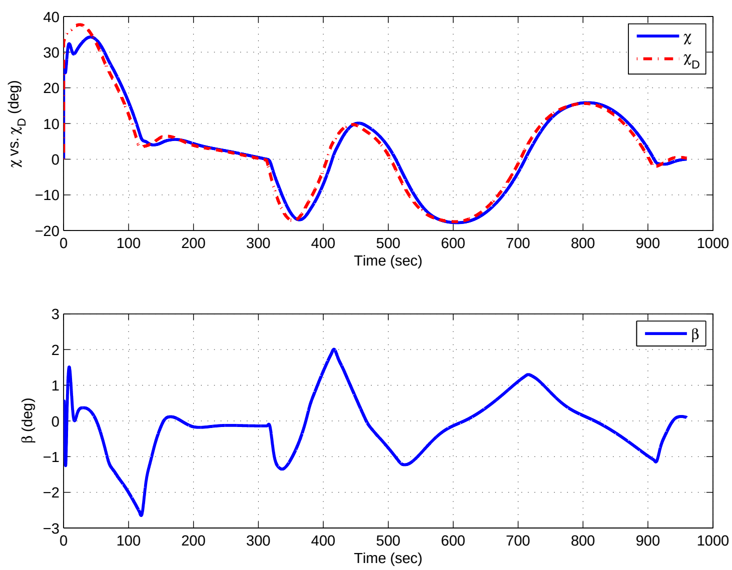

(b) Curved path case

Figure 7: Course angle (desired versus true) and drift angle from the simulations.

$e^{-\frac{2}{5}/e} \approx 0.86 > 0$. It is continuous, positive and globally lower bounded. Obviously, the proposed time-varying vector field guidance law satisfies *Property*

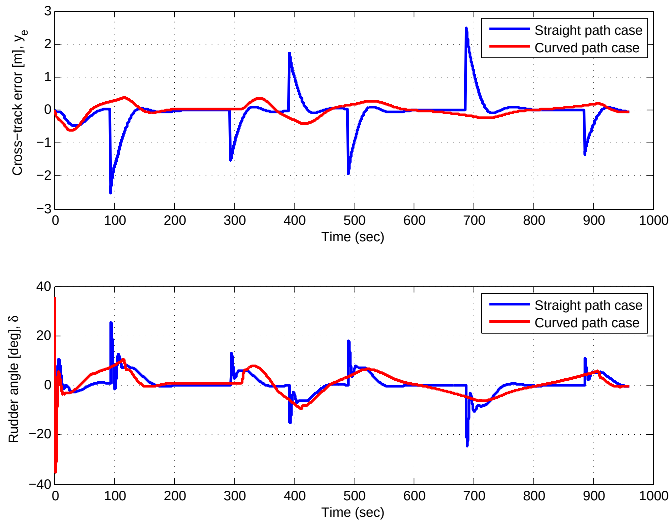

Figure 8: Cross-track error and rudder angle of the underactuated ship following the straight path (blue) and curved path (red) in the presence of ocean currents. In this case, $U_c = 0.4$ m/s, $\beta = 180$ deg, and $\Delta = 2L_{pp}$.

and hence the system equilibrium point is USGES. The predefined parameter, $\Delta = 2L_{pp}$ is chosen twice the ship length. When the ship is moving along the straight-line path a switching mechanism for selecting the next waypoint is needed. For this purpose a circle of acceptance with radius, $R = 2L_{pp}$ around the waypoints is chosen as suggested in reference [6].

$$\psi_d \quad = \gamma_p - \operatorname{sgn}(y_e) \tan^{-1}\left(\left(\frac{|y_e|}{\Delta}\right)^{0.4|y_e|+1}\right) - \beta \tag{43}$$

Figure 5 shows the trajectory of the ship during path following for straight lines and a curved path. As shown in the figure, the ship can follow the straight-line path and curved path in the presence of an ocean current.

In Figure 6, the heading angle and surge speed (desired versus true) are presented. For both cases, the heading autopilot has excellent performance. The sway speed is also shown in Figure 6, for curved-path path following, the fluctuation of sway speed is smaller. The course angles (desired versus true) as well as the crab angle, are plotted in Figure 7. For curved-path path-following, the resulted crab angle is smoother and has smaller fluctuations compared with the straight-line path following. Figure 8 shows the cross-track errors and rudder angles during straight-line path following and curved path following. As shown in the above figure, the curved path following controller has better performance and resulted in smaller cross-track errors compared with the straight-line path-following case, and a smoother rudder angle was deflected when the ship following the curved path.

7. Conclusions

This paper presented a nonlinear time-varying vector field guidance law for path following, which is proven to be uniform semiglobal exponential stable (USGES). The main result was formulated as a theorem, which uses nonlinear cascaded stability theory. In order to obtain a cascaded system structure, a Lyapunov-based sliding mode control has been used for heading autopilot design. The heading controller renders the equilibrium point of the heading error globally exponentially stable (GES). The heading autopilot system together with the time-varying vector field guidance law forms a nonlinear cascade. Using Lyapunov stability theory for nonlinear cascaded systems, we were then able to show USGES.

To evaluate the performance and robustness of the total system, a 3-DOF (surge, sway and yaw) nonlinear mathematical model of an underactuated tanker was considered in a simulation study. For this purpose the mathematical model of the Esso Osaka was used. This ship has been modeled with great accuracy using model tests and this gave confidence in the results. The waypoints were specified by the operator, and the desired paths were generated by connecting all the waypoints using straight line segments and cubic Hermite spline interpolation, respectively. Both straight-line and curved-line path following in the presence of an ocean current were considered. The simulations showed that the proposed time-varying vector field guidance law is capable of following the predefined paths independent of if they are represented as straight lines or curves. The time-varying guidance law can also be applied to other vehicles e.g. autonomous vehicles such as unmanned ground vehicles (UGVs), autonomous underwater vehicles (AUVs), unmanned aerial vehicles (UAVs), just to mention a few.

Acknowledgment

This work was performed within the Strategic Research Plan of the Centre for Marine Technology and Ocean Engineering (CENTEC), which is financed by Portuguese Foundation for Science and Technology (Fundação para a Ciência e Tecnologia-FCT)under contract UID/Multi/00134/2013 - LISBOA-01-0145-FEDER-007629. This work is a contribution to the project M&MSHIPS - Maneuvering & Moored SHIPS in ports (PTDC/EMSTRA/5628/2014) funded by FCT. It was also supported in part by the Research Council of Norway through the Centres of Excellence funding scheme, Project number 223254 – NTNU AMOS. The first author is grateful to Prof. Asgeir Johan Sørensen, who is the director of the Centre for autonomous marine operations and systems (NTNU AMOS), for generous support during the visit.

References

[1] M. Breivik, T. I. Fossen, Guidance laws for autonomous underwater vehicles, in: Underwater vehicles, InTech, 2009, pp. 51–76.

[2] T. I. Fossen, A. M. Lekkas, Direct and indirect adaptive integral line-of-sight path-following controllers for marine craft exposed to ocean currents, International Journal of Adaptive Control and Signal Processing 31 (4) (2017) 445–463.

[3] M. Breivik, T. I. Fossen, Path following for marine surface vessels, in: Oceans '04 MTS/IEEE Techno-Ocean '04 (IEEE Cat. No.04CH37600), Vol. 4, IEEE, 2004, pp. 2282–2289.

[4] M. Breivik, V. E. Hovstein, T. I. Fossen, Straight-line target tracking for unmanned surface vehicles, Modeling, Identification and Control 29 (4) (2008) 131–149.

[5] R. Yanushevsky, Guidance of unmanned aerial vehicles, Taylor & Francis, 2011.

[6] T. I. Fossen, Handbook of marine craft hydrodynamics and motion control, John Wiley & Sons, 2011.

[7] G. V. Raffo, M. G. Ortega, F. R. Rubio, Path tracking of a uav via an underactuated control strategy, European Journal of Control 17 (2) (2011) 194 – 213.

[8] F. M. Barbosa, L. B. Marcos, M. M. da Silva, M. H. Terra, V. Grassi, Robust path-following control for articulated heavy-duty vehicles, Control Engineering Practice 85 (2019) 246 – 256.

[9] Z. Zheng, W. Huo, Z. Wu, Autonomous airship path following control: Theory and experiments, Control Engineering Practice 21 (6) (2013) 769 – 788.

[10] T. I. Fossen, K. Y. Pettersen, R. Galeazzi, Line-of-sight path following for dubins paths with adaptive sideslip compensation of drift forces, IEEE Transactions on Control Systems Technology 23 (2) (2015) 820–827.

[11] C. Liu, J. Sun, Z. Zou, Integrated line of sight and model predictive control for path following and roll motion control using rudder, Journal of Ship Research 59 (2) (2015) 99–112.

[12] S. Moe, K. Y. Pettersen, T. I. Fossen, J. T. Gravdahl, Line-of-sight curved path following for underactuated usvs and auvs in the horizontal plane under the influence of ocean currents, in: 24th Mediterranean Conference onControl and Automation (MED), IEEE, 2016, pp. 38–45.

[13] S. Moe, K. Y. Pettersen, Set-based line-of-sight (los) path following with collision avoidance for underactuated unmanned surface vessels under the influence of ocean currents, in: IEEE Conference on Control Technology and Applications (CCTA), IEEE, 2017, pp. 241–248.

[14] E. Kelasidi, P. Liljebäck, K. Y. Pettersen, J. T. Gravdahl, Integral line-of-sight guidance for path following control of underwater snake robots: theory and experiments, IEEE Transactions on Robotics 33 (3) (2017) 610–628.

[15] H. T. Xu, C. Guedes Soares, An optimized energy-efficient path following algorithm for underactuated marine surface ship model, The International Journal of Maritime Engineering 160 (A4) (2018) A413–A423.

[16] A. M. Lekkas, T. I. Fossen, A time-varying lookahead distance guidance law for path following, IFAC Proceedings Volumes 45 (27) (2012) 398–403.

[17] L. Moreira, T. I. Fossen, C. Guedes Soares, Path following control system for a tanker ship model, Ocean Engineering 34 (14) (2007) 2074–2085.

[18] E. Børhaug, A. Pavlov, K. Y. Pettersen, Integral los control for path following of underactuated marine surface vessels in the presence of constant ocean currents, in: 47th IEEE Conference on Decision and Control, IEEE, 2008, pp. 4984–4991.

[19] W. Caharija, M. Candeloro, K. Y. Pettersen, A. J. Sørensen, Relative velocity control and integral los for path following of underactuated surface vessels, IFAC Proceedings Volumes 45 (27) (2012) 380–385.

[20] A. M. Lekkas, T. I. Fossen, Integral los path following for curved paths based on a monotone cubic hermite spline parametrization, IEEE Transactions on Control Systems Technology 22 (6) (2014) 2287–2301.

[21] K. D. Do, J. Pan, Z.-P. Jiang, Robust adaptive control of underactuated ships on a linear course with comfort, Ocean Engineering 30 (17) (2003) 2201–2225.

[22] K. D. Do, J. Pan, Global robust adaptive path following of underactuated ships, Automatica 42 (10) (2006) 1713–1722.

[23] K. D. Do, J. Pan, Underactuated ships follow smooth paths with integral actions and without velocity measurements for feedback: theory and experiments, IEEE transactions on control systems technology 14 (2) (2006) 308–322.

[24] H. Khalil, Nonlinear systems, vol. 3, Prentice Hall, 2002.

[25] A. Lora, E. Panteley, Cascaded nonlinear time-varying systems: analysis and design, Advanced topics in control systems theory (2005) 23–64.

[26] T. I. Fossen, K. Y. Pettersen, On uniform semiglobal exponential stability (usges) of proportional line-of-sight guidance laws, Automatica 50 (11) (2014) 2912–2917.

[27] O. Sordalen, O. Egeland, Exponential stabilization of nonholonomic chained systems, IEEE transactions on automatic control 40 (1) (1995) 35–49.

[28] K. Y. Pettersen, E. Lefeber, Way-point tracking control of ships, in: Proceedings of the 40th IEEE Conference on Decision and Control, Vol. 1, IEEE, 2001, pp. 940–945.

[29] E. Børhaug, K. Y. Pettersen, Cross-track control for underactuated autonomous vehicles, in: Proceedings of the 44th IEEE Conference on Decision and Control, IEEE, 2005, pp. 602–608.

[30] E. Fredriksen, K. Y. Pettersen, Global κ-exponential way-point maneuvering of ships: Theory and experiments, Automatica 42 (4) (2006) 677–687.

[31] A. Chaillet, A. Loría, Uniform global practical asymptotic stability for time-varying cascaded systems*, European Journal of Control 12 (6) (2006) 595 – 605.

[32] K. Y. Pettersen, Lyapunov sufficient conditions for uniform semiglobal exponential stability, Automatica 78 (2017) 97–102.

[33] D. A. Lawrence, E. W. Frew, W. J. Pisano, Lyapunov vector fields for autonomous unmanned aircraft flight control, Journal of Guidance, Control, and Dynamics 31 (5) (2008) 1220–1229.

[34] Y. Wang, X. Wang, S. Zhao, L. Shen, Vector field based sliding mode control of curved path following for miniature unmanned aerial vehicles in winds, Journal of Systems Science and Complexity 31 (1) (2018) 302–324.

[35] D. R. Nelson, D. B. Barber, T. W. McLain, R. W. Beard, Vector field path following for miniature air vehicles, IEEE Transactions on Robotics 23 (3) (2007) 519–529.

[36] H. T. Xu, C. Guedes Soares, Vector field path following for surface marine vessel and parameter identification based on ls-svm, Ocean Engineering 113 (2016) 151–161.

[37] H. Xu, V. Hassani, C. Guedes Soares, Uncertainty analysis of the hydrodynamic coefficients estimation of a nonlinear manoeuvring model based on planar motion mechanism tests, Ocean Engineering 173 (2019) 450–459.

[38] W. Caharija, K. Y. Pettersen, P. Calado, J. Braga, A comparison between the ilos guidance and the vector field guidance, IFAC-PapersOnLine 48 (16) (2015) 89–94.

[39] T. I. Fossen, A survey on nonlinear ship control: from theory to practice, IFAC Proceedings Volumes 33 (21) (2000) 1 – 16, 5th IFAC Conference on Manoeuvring and Control of Marine Craft (MCMC 2000), Aalborg, Denmark, 23-25 August 2000.

[40] S.-R. Oh, J. Sun, Path following of underactuated marine surface vessels using line-of-sight based model predictive control, Ocean Engineering 37 (2) (2010) 289 – 295.

[41] J. Guerrero, J. Torres, V. Creuze, A. Chemori, Trajectory tracking for autonomous underwater vehicle: An adaptive approach, Ocean Engineering 172 (2019) 511 – 522.

[42] C. Yu, X. Xiang, P. A. Wilson, Q. Zhang, Guidance-error-based robust fuzzy adaptive control for bottom following of a flight-style auv with saturated actuator dynamics, IEEE Transactions on Cybernetics (2019) 1–13.

[43] X. Xiang, C. Yu, L. Lapierre, J. Zhang, Q. Zhang, Survey on fuzzy-logic-based guidance and control of marine surface vehicles and underwater vehicles, International Journal of Fuzzy Systems 20 (2) (2018) 572–586.

[44] M. E. N. Sørensen, M. Breivik, Comparing nonlinear adaptive motion controllers for marine surface vessels, IFAC-PapersOnLine 48 (16) (2015) 291–298.

[45] A. Alessandri, S. Donnarumma, M. Martelli, S. Vignolo, Motion control for autonomous navigation in blue and narrow waters using switched controllers, Journal of Marine Science and Engineering 7 (6).

[46] C. Samson, Path following and time-varying feedback stabilization of a wheeled mobile robot, in: Proceedings of the international conference on advanced robotics and computer vision, Vol. 13, 1992, pp. 1–1.

[47] H. Xu, M. Hinostroza, V. Hassani, C. Guedes Soares, Real-time parameter estimation of a nonlinear vessel steering model using a support vector machine, Journal of Offshore Mechanics and Arctic Engineering 141 (6) (2019) 061606.

[48] L. P. Perera, C. Guedes Soares, Lyapunov and hurwitz based controls for input–output linearisation applied to nonlinear vessel steering, Ocean Engineering 66 (2013) 58–68.

[49] J.-J. E. Slotine, W. Li, Applied nonlinear control, Prentice hall Englewood Cliffs, NJ, 1991.

[50] S. P. Bhat, D. S. Bernstein, A topological obstruction to continuous global stabilization of rotational motion and the unwinding phenomenon, Systems & Control Letters 39 (1) (2000) 63–70.

[51] T. A. Johansen, T. I. Fossen, The exogenous kalman filter (xkf), International Journal of Control 90 (2) (2017) 161–167.

[52] S. Fossen, T. I. Fossen, exogenous kalman filter (xkf) for visualization and motion prediction of ships using live automatic identification system (ais) data.

[53] D. Shevitz, B. Paden, Lyapunov stability theory of nonsmooth systems, IEEE Transactions on automatic control 39 (9) (1994) 1910–1914.

[54] Q. Wu, S. Onyshko, N. Sepehri, A. Thornton-Trump, On construction of smooth lyapunov functions for non-smooth systems, International Journal of Control 69 (3) (1998) 443–457.

[55] A. F. Filippov, Differential equations with discontinuous righthand sides, Springer Science & Business Media, 1988.

[56] A. F. Filippov, Differential equations with discontinuous right-hand side, Matematicheskii sbornik 93 (1) (1960) 99–128.

[57] E. Panteley, A. Loria, On global uniform asymptotic stability of nonlinear time-varying systems in cascade, Systems & Control Letters 33 (2) (1998) 131–138.

[58] E. Panteley, E. Lefeber, A. Loria, H. Nijmeijer, Exponential tracking control of a mobile car using a cascaded approach, IFAC Proceedings Volumes 31 (27) (1998) 201–206.

[59] E. Panteley, A. Loría, A. Sokolov, Global uniform asymptotic stability of cascaded non-autonomous non-linear systems: Application to stabilisation of a diesel engine, European Journal of Control 5 (1) (1999) 107 – 115.

[60] W. Y. Hwang, Application of system identification to ship maneuvering, Ph.D. thesis, Massachusetts Institute of Technology (1980).

[61] H. T. Xu, M. Hinostroza, C. Guedes Soares, Estimation of hydrodynamic coefficients of a nonlinear manoeuvring mathematical model with free-running ship model tests, The International Journal of Maritime Engineering 160 (A3) (2018) A213–A225.